Pattern formation in a surface chemical reaction with global delayed feedback

M. Bertram and A. S. Mikhailov
Fritz-Haber-Institut der Max-Planck-Gesellschaft, Faradayweg 4-6, 14195 Berlin, Germany
(Received 8 December 2000; published 14 May 2001)

We consider effects of global delayed feedback on anharmonic oscillations in the reaction-diffusion model of the CO oxidation reaction on a Pt(110) single-crystal surface. Depending on the feedback intensity and the delay time, we find that various spatiotemporal patterns can be induced. These patterns are characterized using a transformation to phase and amplitude variables designed for anharmonic oscillations. Typical feedback-induced patterns represent traveling phase flips, asynchronous oscillations, and dynamical clustering. Three different types of cluster patterns are identified: amplitude clusters, phase clusters, and cluster turbulence. For phase clusters, two different front instabilities are possible. A pitchfork bifurcation leads to propagation of cluster fronts. An instability of the state of phase balance results in spatial front oscillations.

DOI: 10.1103/PhysRevE.63.066102 PACS number(s): 82.40.Np, 82.40.Bj, 05.45.Xt

I. INTRODUCTION

Spatiotemporal pattern formation in spatially extended systems has been extensively studied during the last two decades [1–3]. Currently, there is a growing interest in controlling and engineering pattern formation in such high-dimensional nonequilibrium systems. The main objectives are the control of spatiotemporal chaos and the induction and stabilization of regular patterns. To achieve these goals, different approaches have been proposed.

Various complex reaction-diffusion patterns can be induced and turbulence can be suppressed by means of periodic external forcing [4–8]. Pattern formation in such systems can also be controlled by feedbacks, where the forcing signal is not fixed, but adjusted to the current state of the medium. Feedback techniques were originally designed for the control of dynamical systems with only a few degrees of freedom [9–11], but later extended for the application to high-dimensional systems governed by partial differential equations [12–21,50] . Some of the proposed techniques require spatially resolved access to the medium under control, because the feedback is applied locally or the signal variation is continuous in space. In contrast to such spatially resolved feedback methods, the controls based on a global feedback act on a single parameter that affects the dynamics of the entire medium. Global feedbacks previously were employed to suppress turbulent states in fluids [22], plasma [23], and semiconductors [24], and recently used to induce cluster patterns in chemical systems [25,26]. Other studies were devoted to the global control of spiral waves in excitable chemical media [27,28], and to the stabilization of traveling spots by global feedback [29,30].

For oscillatory reaction-diffusion systems, a form of delayed global feedback useful both for the effective suppression of turbulence and for the generation of new spatiotemporal patterns has previously been proposed [17]. In this method the forcing signal is directly proportional to the past integral state of the medium. The feedback loop can be easily implemented experimentally without the knowledge of the governing equations and, in the case of unstable conditions, it automatically adjusts to a parameter drift of the system. The delay can be used to effectively modify the phase relation between the control signal and the oscillating pattern. The related research was so far focused on the normal form approach [17,31–33] that is valid close to the soft onset of oscillations.

In this paper we apply this kind of delayed global feedback to a realistic model describing the catalytic chemical reaction of carbon monoxide oxidation on a platinum single-crystal surface. This system is not close to a supercritical Hopf bifurcation and the oscillations are not harmonic. We also present a technique developed for the analysis of reaction-diffusion patterns with anharmonic oscillation dynamics. The objective is to extend the amplitude and phase description used in the normal form approach to problems involving anharmonic oscillation dynamics.

The paper is organized as follows: The considered system and the feedback method are introduced in Sec. II. In Sec. III a transformation of chemical concentrations into amplitude and phase variables is described. Simulation results for one-dimensional media are presented in Sec. IV, with an emphasis on the analysis of different front instabilities of cluster patterns. In Sec. V results of numerical simulations in two dimensions are reported. The paper ends with a discussion of the obtained results.

II. FORMULATION OF THE PROBLEM

The development of spatially resolving techniques such as photoemission electron microscopy (PEEM) [34] has made surface chemical reactions a convenient system to probe various aspects of nonequilibrium spatiotemporal pattern formation. Among surface chemical reactions, the catalytic oxidation of carbon monoxide at platinum single-crystal surfaces has been studied most extensively and is best understood. The observed nonequilibrium phenomena include rate oscillations and spatiotemporal patterns, such as rotating spiral waves, target patterns, standing waves, and turbulence [35,36]. The phenomena are similar to those observed in the Belousov-Zhabotinsky reaction [37], but the reaction mechanism is comparatively simple and involves only a few species. The reaction follows the Langmuir-Hinshelwood (LH) scheme

$$* + \mathrm{CO} \rightleftharpoons \mathrm{CO_{ad}},$$

TABLE I. Parameters of the model.

k_1	$3.14\times10^5\ \mathrm{s}^{-1}\,\mathrm{mbar}^{-1}$	Impingement rate of CO
k_2	$10.21\ \mathrm{s}^{-1}$	CO desorption rate
k_3	$283.8\ \mathrm{s}^{-1}$	Reaction rate
k_4	$5.860\times10^5\ \mathrm{s}^{-1}\,\mathrm{mbar}^{-1}$	Impingement rate of O_2
k_5	$1.610\ \mathrm{s}^{-1}$	Phase transition rate
s_{CO}	1.0	CO sticking coefficient
$s_{\mathrm{O},1x1}$	0.6	Oxygen sticking coefficient on the 1x1 phase
$s_{\mathrm{O},1x2}$	0.4	Oxygen sticking coefficient on the 1x2 phase
u_0, δu	0.35, 0.05	Parameters for the structural phase transition
D	$40\ \mu\mathrm{m}^2\,\mathrm{s}^{-1}$	CO diffusion coefficient
p_{O_2}	9.00×10^{-5} mbar	O_2 partial pressure
p_{CO}	4.15×10^{-5} mbar	CO partial pressure

$$2^* + \mathrm{O}_2 \rightarrow 2\,\mathrm{O}_{\mathrm{ad}},$$

$$\mathrm{CO}_{\mathrm{ad}} + \mathrm{O}_{\mathrm{ad}} \rightarrow 2^* + \mathrm{CO}_2.$$

Here, * denotes a free adsorption site on the catalytic surface. Due to a high energy barrier in the gas phase, CO and oxygen molecules have to (dissociatively) adsorb before the reaction. Produced carbon dioxide almost immediately desorbs into the gas phase leaving again free space for adsorption. The system is maintained far from thermodynamic equilibrium by constant supply of fresh reactants and removal of the product. Experiments performed in an UHV chamber under isothermal low-pressure conditions ($p < 10^{-3}$ mbar) have shown an asymmetric inhibition of adsorption: preadsorbed CO molecules inhibit oxygen adsorption but not vice versa. The LH mechanism in combination with the asymmetric inhibition of adsorption leads to a bistability between the mainly oxygen-covered, reactive state and the nonreactive CO-covered state.

Temporal rate oscillations in the CO oxidation require an additional mechanism. On a Pt(110) single-crystal surface the mechanism for rate oscillations and related oscillations of the CO and oxygen coverage is provided by an adsorbate-driven structural phase transition in the top substrate layer. The clean Pt(110) surface reconstructs into a 1×2 ''missing row'' structure. The reconstruction can be reversibly lifted by adsorbed CO molecules. Oxygen adsorption is stronger on the nonreconstructed 1×1 phase and therefore the phase transition can cause periodic switching between the two states with different catalytic activity.

Spatial coupling in the system is provided by two different mechanisms. Surface diffusion of adsorbed CO molecules gives rise to local coupling between neighbored sites. Spatial coupling via the gas phase acts as a consequence of the mass balance in the reaction. Since the mean free path in the gas phase is typically large in comparison to the chamber dimensions, local partial pressure variations that result from the consumption of the educts by the reaction quickly extend to the whole system. Therefore, the gas-phase coupling is global. The interplay between local and global coupling experimentally was shown to lead to phenomena such as synchronous oscillations [38] and standing waves [35,39].

The first detailed mathematical model of the CO oxidation reaction on Pt(110) has been developed by Krischer, Eiswirth, and Ertl [40]. Later a modified version of this model that included diffusion was used to study pattern formation for bistable, excitable, and oscillatory kinetics. These studies demonstrated very good qualitative, sometimes even quantitative agreement with the experimental observations [41,42]. Experiments with oxygen island conversion could be quantitatively reproduced when a subsurface oxygen species was included in the model [43]. Other studies that concentrated on pattern formation under global coupling revealed a variety of structures including cluster patterns and standing waves [39,44–46].

In the present study a three-variable form of this model is used. The variables u and v denote the surface coverage of carbon monoxide and oxygen, respectively. The variable w is related to the local structural state of the surface and denotes the local fraction of the surface area found in the nonreconstructed 1×1 structure. All three properties can vary in the interval from 0 to 1. The equations are

$$\frac{\partial u}{\partial t} = k_1 s_{\mathrm{CO}} p_{\mathrm{CO}} (1-u^3) - k_2 u - k_3 u v + D\nabla^2 u, \qquad (1)$$

$$\frac{\partial v}{\partial t} = k_4\, p_{\mathrm{O}_2} [\, s_{\mathrm{O},1x1} w + s_{\mathrm{O},1x2}(1-w)](1-u-v)^2 - k_3 u v, \qquad (2)$$

$$\frac{\partial w}{\partial t} = k_5 \left(\frac{1}{1+\exp\left(\dfrac{u_0-u}{\delta u}\right)} - w \right). \qquad (3)$$

For explanation of the parameters see Table I. Equations (1)–(3) take into account the reaction, asymmetric inhibition of adsorption, desorption of CO, the phase transition of the platinum surface and surface diffusion of adsorbed CO molecules. Oxygen desorption and diffusion are negligible at the

considered temperature ($T=545$ K). For simplicity, surface roughening, faceting, and formation of subsurface oxygen are not taken into account in the present study.

The aim of our study is to show that pattern formation in the CO oxidation reaction can be effectively controlled and various additional patterns can be induced by employing delayed global feedback control. Experiments employing such a feedback loop are currently in progress. The suggested setup is the following: A feedback loop is artificially applied to the reaction by means of continuous computer-controlled variation of one of the partial pressures in the chamber. The external pressure variations globally affect the dynamics on the entire catalytic surface. A spatially resolving technique, such as PEEM, is used to monitor the coverage patterns forming in the active surface area. For the generation of the control signal the spatial average of the measured PEEM intensity is simultaneously computed. The continuous signal that is the difference between the average and a reference intensity, multiplied by a factor determining the feedback intensity, is applied back to the reaction with a certain artificially introduced delay. The delay can be adjusted to control the phase relation between the oscillating pattern and the feedback signal. The idea is that different patterns can be induced simply by variation of the two computer-controlled feedback parameters, the feedback intensity and the delay time.

As already noted, the reaction consumes reactants from the gas phase and therefore an intrinsic global gas-phase coupling is always additionally present (some of its effects have previously been investigated [44–46]). In our investigations, the intrinsic gas-phase coupling will be neglected because it is weak as compared with the typical feedback intensity levels that can be achieved by modulating the gas supply rates.

To approximately model the suggested global feedback experiment, we assume in this paper that the CO partial pressure p_{CO} in Eq. 1 is not constant but varies as

$$p_{\mathrm{CO}}(t)=p_{\mathrm{CO}}^{0}-\mu\,[\,\overline{u}(t-\tau)-u_{\mathrm{ref}}], \tag{4}$$

where $\overline{u}(t)=1/S\int_S u(x,t)\,dx$ denotes the spatial average of the CO coverage u at time t. The parameter μ specifies the feedback intensity, τ is the delay, and p_{CO}^{0} is the CO partial pressure for vanishing feedback, $\mu=0$. Hence the CO partial pressure in Eq. 1 is adjusted according to the difference between the integral delayed CO coverage $\overline{u}(t-\tau)$ and its reference value u_{ref}. The reference value is chosen as the CO coverage in the unstable steady state in absence of feedback. In the limit of a small delay τ the feedback acts towards stabilization of the target state $\overline{u}=u_{\mathrm{ref}}$.

In both one- and two-dimensional numerical simulations of model (1)–(4), a second-order finite difference scheme is used for the approximation of the Laplacian operator with a grid resolution $\Delta x=4$ μm. The resulting set of ordinary differential equations is solved using an explicit Euler scheme with a fixed time step $\Delta t=0.001$. The boundary conditions are either no-flux (Neumann) or periodic, and different initial conditions are employed. Unless stated otherwise, the system size is 0.8 mm for one-dimensional and 0.8×0.8 mm^2 for two-dimensional simulations. Long integration times $t>5000$ s ensure that transients have decayed at the end of each calculation. The model parameters (Table I) are chosen in such a way that the system performs anharmonic limit-cycle oscillations that are stable in absence of feedback. In our numerical study we keep constant all parameters, except the feedback intensity μ and the delay τ that will be systematically varied.

III. PATTERN CHARACTERIZATION

A powerful theoretical approach to understand spatiotemporal pattern formation is provided by the normal form theory. The derivation of an amplitude equation leads to a simplified description of the universal properties of a system close to a bifurcation point [1,47] . The amplitude equation of a field of diffusively coupled Hopf oscillators valid near the onset of oscillations is the complex Ginzburg-Landau equation (CGLE). The CGLE describes harmonic oscillations in terms of their amplitude modulus and phase. The oscillations observed in real experimental situations are usually anharmonic, so that the system is not close to a Hopf bifurcation. Nonetheless, the normal form theory is often applied to interpret the experimental data even in such cases. Indeed, the predictions of the CGLE may remain qualitatively correct in a larger neighborhood of the bifurcation.

It would be convenient to have the amplitude and the phase variable also defined for anharmonic oscillations, in such a way that they correspond to the amplitude and the phase of quasiharmonic oscillations in the normal form theory. It should be noted that the local phases of general anharmonic oscillations were first introduced by Kuramoto [1] in his analysis of phase dynamics. However, only small amplitude deviations from the nonperturbed limit cycle were then considered.

A recent approach to such a variable transformation was undertaken by employing a frequency demodulation technique to filter relevant information from numerical and experimental data [8]. This technique uses a finite width frequency filter to extract the behavior of a certain mode in the patterns. The complex Fourier coefficients of this mode are computed from the time series at various locations in the patterns to provide a local phase and amplitude characterization of the dynamics. This technique is efficient when the majority of the dynamical power is concentrated in a single mode, but it is also limited to this case. The time-resolved description of oscillatory behavior requires extensive data processing and is only achievable for sufficiently slow pattern evolutions.

The variable transformation we present in this paper follows a different idea. It is an empirical method to transform a pair of model variables into an amplitude and a phase after computational modeling. We cannot ensure that this transformation is generally applicable. However, when certain conditions on the spatiotemporal dynamics of the pattern under analysis are fulfilled, the method turns out to be a useful tool for the time-resolved characterization of patterns involving anharmonic dynamics, as shown in the following sections.

When a system has periodic oscillatory dynamics in ab-

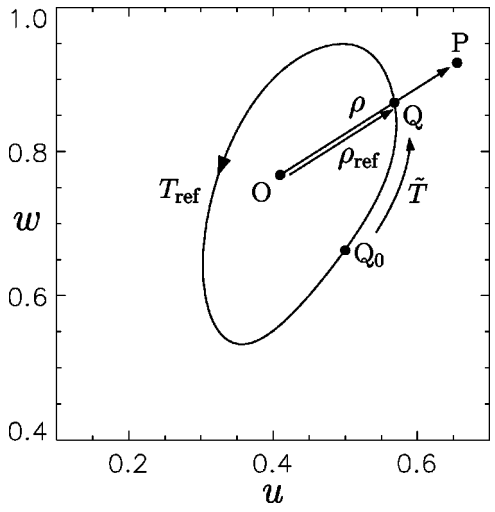

FIG. 1. Definition of the amplitude $R=\rho/\rho_{\mathrm{ref}}$ and phase $\phi=2\pi\tilde{T}/T_{\mathrm{ref}}$ variables for anharmonic oscillations.

sence of spatial coupling, visualization of two variables is sufficient to capture the relevant dynamical features. In the projection plane of these two variables, the limit cycle yields a closed trajectory. We choose the projection variables in such a way that this trajectory has no self-intersection. We shall further assume that, when spatial coupling is eventually introduced, the local oscillations in the medium are not greatly different from those that correspond to the uniform limit cycle, except for relatively small localized areas where strong deviations from the uniform attractor may still occur. The projected uniform limit cycle can therefore be used as a reference for the characterization of dynamics in a spatiotemporal pattern.

The employed variable transformation is illustrated in Fig. 1. Suppose that u and w are the projection variables and the reference limit cycle projection is the closed orbit shown in Fig. 1. We want to define for *any* state P with coordinates (u,w) in the projection plane a pair of new variables R and ϕ that can be interpreted as an amplitude and a phase corresponding to this local state of the system. To do this, we first choose some point O inside the reference orbit and take it as the coordinate origin in the projection plane. Hence, any point P is characterized by a radius vector of length $\rho=\overline{\mathrm{OP}}$. We notice the point Q where this radius (or it extension) intersects with the chosen orbit. The length $\rho_{\mathrm{ref}}=\overline{\mathrm{OQ}}$ determines the reference radius for the point P. Next we mark some ''initial'' point Q_0 on the orbit and determine the time $\tilde{T}$ needed to reach point Q along the reference cycle. The amplitude and the phase are then defined as $R=\rho/\rho_{\mathrm{ref}}$ and $\phi=2\pi\tilde{T}/T_{\mathrm{ref}}$, where T_{ref} is the period of the reference limit cycle.

Note that according to this definition, the amplitude is $R=1$ as long as the system stays on the reference limit cycle. Moreover, for the motion corresponding to the reference limit cycle, the phase ϕ increases at a constant velocity with time and changes by 2π after each cycle period. When local oscillations are nearly harmonical and the reference orbit is a circle with point O in its center, the above definition yields the usual phase and amplitude variables. The coordinate origin O is best chosen as the unstable uniform steady state of the system to guarantee that a local suppression of oscillations indeed corresponds to a vanishing amplitude R.

Below we apply this empirical amplitude-phase description to qualitatively interpret spatiotemporal patterns obtained in our numerical simulations of the CO oxidation reaction with artifical global feedback. To obtain the reference orbit we shall use the projection of uniform oscillations in the model on the plane with the variables u and w, representing CO coverage and the fraction of the nonreconstructed surface area.

It should be noted that when the feedback Eq. (4) is present, it may significantly affect the shape of uniform oscillations. Therefore we employ different reference orbits for different feedback parameters by generating a new reference cycle following each fixed parameter simulation of the model Eqs. (1)–(4). This is done by an additional numerical simulation of the model Eqs. (1)–(3) in absence of diffusion $(D=0)$, where the feedback signal generated previously by the full pattern forming system is applied as external p_{CO} forcing. The projection of the resulting attractor is periodic and directly used as reference when the global oscillations in the asymptotic state of the respective full system are periodic. In the examples encountered when the full system generated an aperiodic forcing signal the resulting attractor in the projection plane deviated only slightly from a periodic limit cycle. In those cases the reference limit cycle was chosen as the long-time average of the resulting projected trajectory.

IV. FEEDBACK-INDUCED PATTERNS IN ONE SPACE DIMENSION

We have numerically examined feedback-induced pattern formation in the model described by Eqs. (1)–(4). In this section we present the results of numerical simulations for one-dimensional systems. The model parameters are given in Table I, and the fixed feedback parameters are $p_{\mathrm{CO}}^0=4.15\times10^{-5}$ mbar and $u_{\mathrm{ref}}=0.4097$. Note that the parameters are chosen in such a way that uniform oscillations are stable when the feedback intensity vanishes. Periodic boundary conditions have been used, unless a different condition is specified. The simulations were continued until an asymptotical stable regime was reached after a transient. Multiple simulations at different values of feedback intensity μ and delay time τ have been performed.

The results of our numerical investigations of one-dimensional systems are summarized in Fig. 2. This diagram shows the types of stable regimes reached after transients in the considered system. The delay time is measured in multiples of the natural oscillation period in absence of feedback, $T_0=3.33$ s (note that when feedbacks are operating the actual period of uniform oscillations is feedback dependent and will to some extent differ from T_0). The feedback intensity in Fig. 2 is normalized to the equilibrium CO partial pressure p_{CO}^0 in the reaction chamber in absence of feedback. Note that the ratio μ/p_{CO}^0 yields an estimate of the relative variation of partial pressure caused by such a feedback.

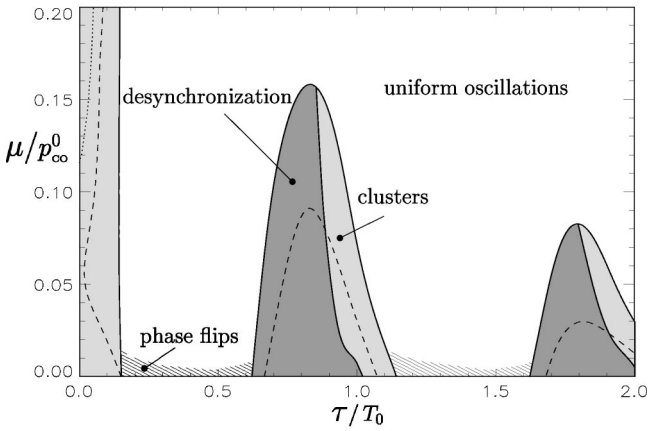

FIG. 2. Existence regions of various feedback-induced patterns in the one-dimensional system: uniform oscillations (white), asynchronous oscillations (dark gray), and cluster patterns (light gray). Phase flips are observed in the hatched regions. The dashed lines mark the borders of the hysteresis of uniform oscillations.

Depending on the delay and intensity, the feedback can maintain uniform oscillations or induce various spatiotemporal patterns. Examining Fig. 2, we see that as the delay is increased, the diagram is approximately repeated at integer multiples of T_0 (this trend is continued at larger delays, not shown in Fig. 2). However, the stability regions of the patterns other than uniform oscillations shrink at larger delays.

Uniform oscillations are found in a large region of the two-parameter plane. The uniform oscillations have strong hysteresis (bold lines show the boundaries where uniform oscillations set on when increasing the feedback intensity, whereas dashed lines indicate the boundaries where such oscillations break down as the feedback intensity is decreased). In the hysteresis regions the final pattern depends on the initial conditions because the uniform attractor coexists here with the attractor of another pattern.

For comparison, we also show by the dotted line in Fig. 2 the boundary where in absence of diffusion the unstable steady state of the system becomes stabilized by the applied feedback (the stabilization takes place at small delays $\tau/T_0 < 0.06$ and large feedback intensities $\mu/p^0_{CO} > 0.11$). In the pattern forming system that includes diffusion the spatially uniform suppression of oscillations on the entire surface is however not observed. Instead, at small delays the system evades the suppression of oscillations through the formation of clusters.

Figure 3 displays three typical examples of different nonuniform feedback-induced patterns. In the pattern shown in Fig. 3(a) the medium is in the uniform state almost anywhere except for a narrow interval with strong spatial variation. As we shall later see, this pattern corresponds to a *phase flip* traveling across the medium. In contrast to this, the pattern in Fig. 3(b) is characterized by a gradual spatial variation extending over the whole medium. We show below that such patterns are found when *desynchronization* through the feedback is taking place. In Fig. 3(c) the pattern consists of large regions with almost uniform distributions separated by narrow interfaces. Such *cluster patterns* are also discussed below.

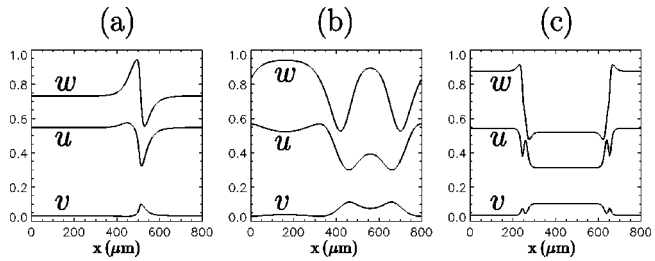

FIG. 3. Feedback-induced coverage patterns: (a) phase flip, (b) asynchronous oscillations, and (c) a cluster pattern. For each pattern the values of the parameters τ/T_0 and μ/p^0_{CO} are, respectively, (a) 0.165, 0.012, (b) 0.781, 0.012, and (c) 0.045, 0.289.

A. Phase flips

As we have already noted, in this paper we consider only the case when uniform oscillations are stable with respect to spontaneous phase modulation in absence of feedback. Depending on the choice of the initial and the boundary conditions, traveling waves (and spiral waves in the two-dimensional system) can still be observed in this case. Sufficiently strong global delayed feedbacks suppress all such structures, so that only uniform oscillations are found inside the blank region in Fig. 2. After a transient, any initial condition eventually leads to uniform oscillations here. The time needed to reach uniform oscillations greatly increases near the instability boundaries of uniform oscillations.

At small feedback intensities corresponding to the hatched areas in Fig. 2, either uniform oscillations or patterns of propagating *phase flips* are found in the simulations, depending on the initial conditions. To produce a phase flip, a simulation is started with a constant phase gradient of 2π across the system. The feedback tends to establish uniform oscillations, but, if it is relatively weak, it cannot achieve this in the whole medium. Thus, a narrow region with strong concentration gradients is formed, see Fig. 3(a). This region travels through the medium.

To analyze the properties of such traveling patterns, we use the variable transformation technique described in Sec. III. After transformation to local phase and amplitude variables, the pattern of a phase flip takes the form displayed in Fig. 4(a). We see that the oscillation phase ϕ undergoes a full rotation of 2π inside the nonuniform region whereas the amplitude R displays only small modulations. The states of the medium on the left and right side of the phase flip differ by a phase shift of 2π only and hence are physically indistinguishable.

A phase portrait of the same structure is shown in Fig. 4(b). Here, the amplitudes and phases of all points along the phase flip are displayed in polar coordinates. The phase ϕ of a point is represented by the polar angle and the amplitude R is the distance to the coordinate origin. The points accumulate in the state corresponding to the uniformly oscillating regions.

Phase flips were first reported for the periodically forced CGLE [4] (see also Ref. [7]) and were systematically inves-

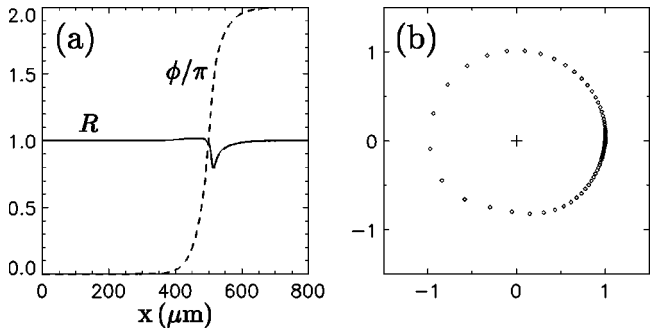

FIG. 4. (a) Spatial dependence of the amplitude R (solid line) and the phase ϕ (dashed line) in a phase flip. The phase portrait (b) shows the same data in polar coordinates. The same parameters as in Fig. 3(a).

tigated for the CGLE in the presence of a global feedback [31,33]. Remarkably, the amplitude and phase plots obtained by the variable transformation in our model with anharmonic oscillations are very similar to the respective plots for the CGLE with global feedback (cf. Fig. 4(a) and Fig. 4 in Ref. [33]).

The previous analytical investigations of phase flips in the CGLE with global feedback have revealed [31,33] that, depending on the feedback parameters, a phase flip can stop and reverse its direction of motion. Following Ref. [31], a phase flip is said to have positive velocity V if the phase is increased by 2π after its passage and the velocity is negative if the phase decreases by 2π behind it. With this in mind, we have numerically examined the dependence of the propagation velocity of phase flips on the delay time τ in the currently investigated model with anharmonic oscillations. As displayed in Fig. 5, the velocity V decreases for higher delays and changes its sign at $\tau/T_0 \approx 0.155$. Another prediction of the study of the CGLE with global feedback is that, as the feedback intensity μ is decreased, the width of the phase flip grows as $\delta x \sim \mu^{-1/2}$ and in the limit $\mu \to 0$ the phase flip transforms into uniform oscillations in a finite system. We have checked that this effect is also observed for phase-flip patterns in the presently considered model.

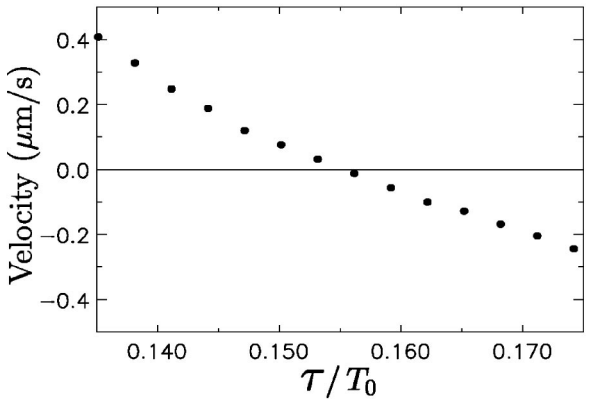

FIG. 5. Dependence of the velocity of phase flips on the delay time. The feedback intensity is constant, $\mu/p_{CO}^0 = 0.012$.

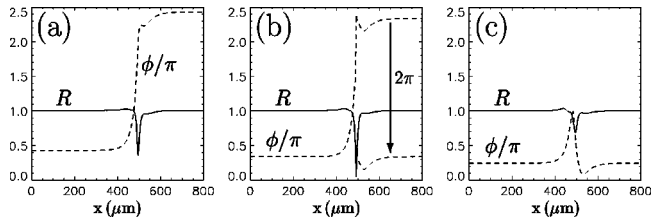

FIG. 6. Destruction of a phase flip by strong global feedback. The time interval between the subsequent snapshots (a)–(c) showing oscillation phases (dashed lines) and amplitudes (solid lines) is 3 seconds. The feedback parameters are $\tau/T_0 = 0.167$ and $\mu/p_{CO}^0 = 0.014$. The initial phase flip was obtained using a slightly smaller feedback intensity $\mu/p_{CO}^0 = 0.012$.

On the other hand, phase flips become unstable in our simulations if the feedback intensity exceeds a certain delay-dependent threshold (see Fig. 2). They dissappear through the formation of an amplitude defect if the feedback intensity is increased beyond the critical value. This process is analyzed in Fig. 6 by means of our amplitude and phase characterization. Before the amplitude defect occurs the phase variation is steepened, see Fig. 6(a). Then at some moment the oscillation amplitude drops down to zero inside the phase flip. When this occurs the phase, which is not defined when the amplitude vanishes, makes a slip of 2π at one side of the defect, as illustrated in Fig. 6(b). After the phase slip, the amplitude slowly approaches unity and the phase variation smears out, eventually giving rise to uniform oscillations. This scenario is in perfect agreement with the disappearance of phase flips in the CGLE under increasing global feedback intensity [33] (the destruction of phase flips by strong external forcing in the CGLE has also been subsequently observed [7]).

B. Asynchronous oscillations

Patterns with smooth spatial gradients of chemical variables can be induced by the feedback in the desynchronization region displayed in Fig. 2. Below the dashed lines in this region, asynchronous patterns develop starting from any initial condition. The duration of the desynchronization process diverges for feedbacks of vanishing intensity. Applying the transformation to local phase and amplitude variables, asymptotic asynchronous patterns established in this regime can be analyzed. Spatial profiles of R and ϕ in such a pattern are shown in Fig. 7(a). We note that only the local oscillation phase ϕ is varying in this pattern, whereas the amplitude R is almost constant. This means that all local oscillations correspond to the same limit cycle. The phase profile shows smooth variation. When the size of the medium was varied in simulations, the pattern always adjusted to the size of the medium, therefore lacking an intrinsic wavelength. In the phase portrait representation of such a pattern all points are distributed on the unit circle, see Fig. 7(b). However, not all possible phases are occupied, and the density of points increases towards the ends of the structure that correspond to the extrema of the phase profile. As time goes on, the structure rotates in the plane with constant velocity.

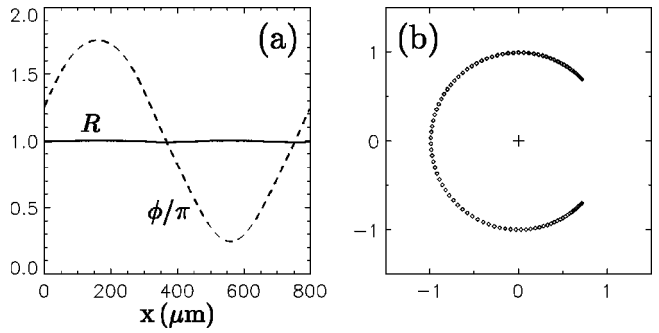

FIG. 7. (a) Spatial dependence of the phase (dashed line) and the amplitude (solid line) and the phase portrait (b) of a pattern of asynchronous oscillations. A slightly perturbed uniform distribution was taken as initial condition. The same parameters as in Fig. 3(b).

Under periodic boundary conditions, the total phase gradient along the pattern always adjusts to an integer multiple of 2π given by the winding number of the initial phase distribution. For a nonzero winding number, the asymptotic spatial profile of the phase ϕ is linear, so that the temporal shift between oscillations at different sites is proportional to their spatial distance. No-flux boundary conditions do not conserve the winding number. In the latter case the final total phase gradient does not exceed 2π.

An important consequence of the spatial desynchronization of oscillations is the accompanying breakdown of the global oscillations that generate the feedback signal. As shown in Fig. 8, the amplitude of the feedback signal decreases as the desynchronization gradually develops in the system. Thus, the global feedback effectively induces its own breakdown. It should be noted that the feedback oscillations do not, however, completely vanish in the asymptotic state. A small remaining feedback signal that compensates the synchronizing tendency of diffusion is needed to maintain the desynchronized state. Such desynchronization phenomena have previously been found in numerical investigations of the CGLE with global feedback [31].

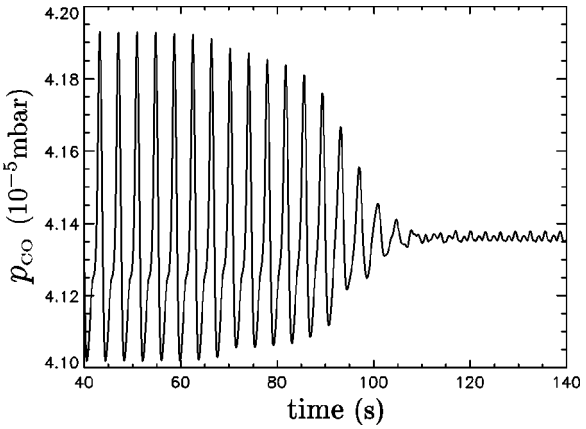

FIG. 8. Breakdown of the feedback-induced CO pressure variations during the desynchronization of initially slightly perturbed uniform oscillations. The feedback parameters are $\tau/T_0=0.781$ and $\mu/p^0_{CO}=0.048$.

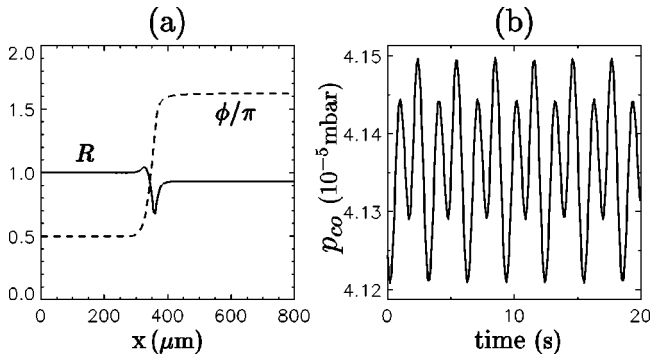

FIG. 9. (a) Phase and amplitude profiles of amplitude clusters. The reference limit cycle for the variable transformation is chosen as the attractor of the cluster state with the higher amplitude. No-flux boundary conditions are used. Frame (b) shows global oscillations corresponding to the pattern in frame (a). The feedback parameters are $\tau/T_0=0.045$ and $\mu/p^0_{CO}=0.072$.

C. Cluster patterns

The third principal mechanism of feedback-induced pattern formation involves clustering of oscillations. The cluster regimes include a variety of qualitatively different patterns. Their common feature is the presence of a small number of synchronized domains, occupied by one of two possible oscillatory states. No intrinsic spatial wavelength of the domains is observed. We divide different cluster solutions into amplitude clusters, phase clusters, and cluster turbulence.

1. Amplitude clusters

In amplitude clusters, not only the oscillation phases ϕ, but also the oscillation amplitudes R are different in the regions occupied by the two different states, as shown in Fig. 9(a). Thus, uniform oscillations within two different clusters correspond to different coexisting limit cycles of equal period. The phase shift between the oscillations in the two cluster states (about 0.88π in the example shown) is constant, but depends on the feedback parameters. At the interface between two stationary cluster domains, the phase ϕ is monotonously increased and the amplitude R undergoes small variations. The total size ratio of the domains that belong to each state is independent of the initial domain sizes and has a characteristic value that changes with the feedback parameters. The difference in the contributions to global oscillations coming from the two clusters results in period-doubled oscillations of the control signal, see Fig. 9(b). Amplitude clusters were previously seen in the simulations of the CGLE with global feedback [33]. They were also investigated in the studies of the CO oxidation reaction under intrinsic gas-phase coupling [44] and similar properties were then found.

2. Phase clusters

Phase clusters are characterized by equal oscillation amplitudes and a constant phase shift between the cluster states. The oscillations in both cluster states correspond now to the same limit cycle, but are of opposite phase. The phase fronts that separate different cluster domains exhibit rich behavior, as demonstrated below. At high feedback intensities, station-

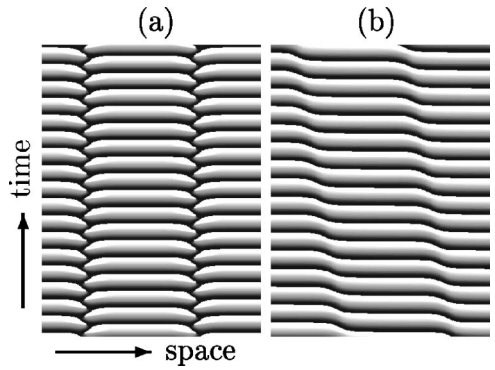

FIG. 10. Phase clusters with (a) stationary (Ising) phase fronts and (b) traveling (Bloch) phase fronts. Both diagrams display the oscillation phase ϕ in a time interval of 50 s. The system size is 0.4 mm. The values of the parameters τ/T_0 and μ/p^0_{CO} are, respectively, (a) 0.105, 0.241, and (b) 0.120, 0.096.

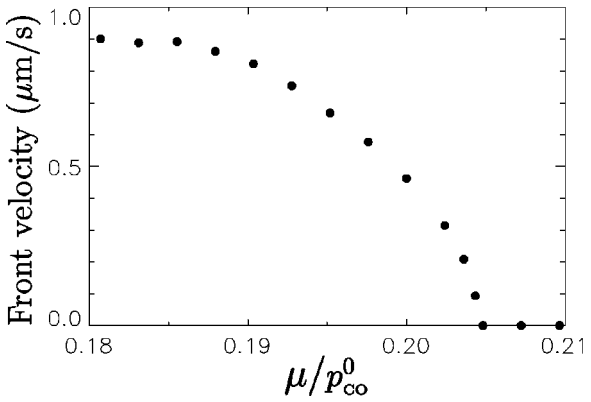

FIG. 11. Long-time average of the phase front velocity in cluster patterns as function of the feedback intensity. The data points were obtained numerically with a system size equal to 0.4 mm. The delay time is kept constant, $\tau/T_0=0.105$.

ary phase clusters prevail, see Fig. 10(a). The asymptotic spatial formation of the domains in such a pattern depends on the initial conditions. However, the total fraction of the medium occupied by the domains of each cluster is balanced, a phenomenon that, following Ref. [26], we call *phase balance*. When a simulation is started with a different initial size ratio, the fronts between the cluster domains slowly drift and finally come to rest in the state of phase balance. As a consequence, the average that generates the feedback signal is periodic and resonantly oscillates with a frequency twice larger than that of the periodic local oscillations inside the cluster domains.

(a) Bifurcation to traveling phase clusters. Stationary phase clusters can undergo a transition to traveling clusters, an example of which is shown in Fig. 10(b). Periodic boundary conditions are necessary for the observation of such propagating patterns, because they preserve the size ratio between the clusters. This transition is related to a symmetry-breaking bifurcation, known as the nonequilibrium Ising-Bloch bifurcation [48] that leads to fronts traveling with constant velocity. The two branches of this pitchfork bifurcation correspond to counter-propagating fronts with equal absolute velocity and opposite sign. The dependence of the absolute velocity of traveling phase clusters on the feedback intensity at a fixed delay is shown in Fig. 11. We see that a bifurcation from stationary (Ising) fronts to traveling (Bloch) fronts occurs when the feedback intensity is decreased.

It is interesting to compare the phase and amplitude properties of oscillations in stationary and traveling phase-cluster patterns. The phase portraits of such patterns are shown in Fig. 12. In the stationary cluster pattern displayed in Fig. 12(a), the two cluster states correspond to the ends of the S-shaped structure where the points accumulate. The other points in this structure correspond to the front that separates the clusters. Note that the S-shaped structure goes through the origin of the plane, i.e., there is a point inside the front where the oscillation amplitude R vanishes. At this point the phase ϕ undergoes a jump by π.

At the transition to traveling Bloch fronts a topological bifurcation is observed in the phase portrait. When the bifurcation occurs, the S-shaped curve splits into two different branches that connect the two cluster states. Farther away from the bifurcation point, the fronts between the cluster states are mapped almost to a circle, as shown in Fig. 12(b). The phase ϕ undergoes a continuous rotation with a total of π when traversing such a Bloch front, whereas R shows only small modulations. By application of the transformation to phase and amplitude variables, we have thus found that the properties of such Ising and Bloch fronts are close to those found for the amplitude equation of oscillatory media under external forcing [48].

(b) Bifurcation to oscillating phase clusters. Furthermore, we have observed another interesting phase front instability, a Hopf bifurcation of a front that separates two clusters. The origin of this bifurcation is an instability of the phase balance that gives rise to periodic oscillations of the cluster size ratio. As a consequence, cluster fronts periodically change their spatial position, see Fig. 13(a). We define the front position as the location within the front where the amplitude R is minimal. The period of the front oscillations comprises several local oscillations.

Figure 14 shows the dependence of the amplitude of front oscillations on the feedback intensity at a constant delay. The bifurcation from a stationary front to an oscillating cluster front occurs when the feedback intensity is decreased. The parabolic fit (solid line in Fig. 14) is in good agreement with

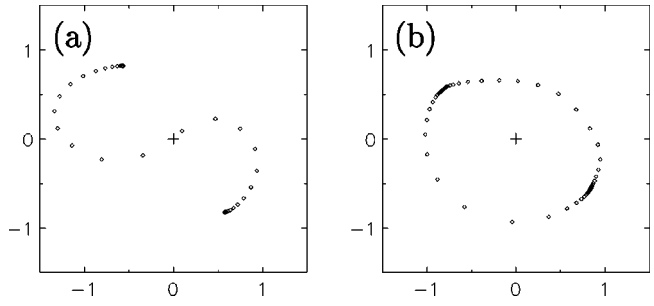

FIG. 12. Phase portraits of cluster patterns with (a) a stationary Ising phase front and (b) traveling Bloch phase fronts. The values of the parameters τ/T_0 and μ/p^0_{CO} are, respectively, (a) 0.045, 0.289, and (b) 0.120, 0.096.

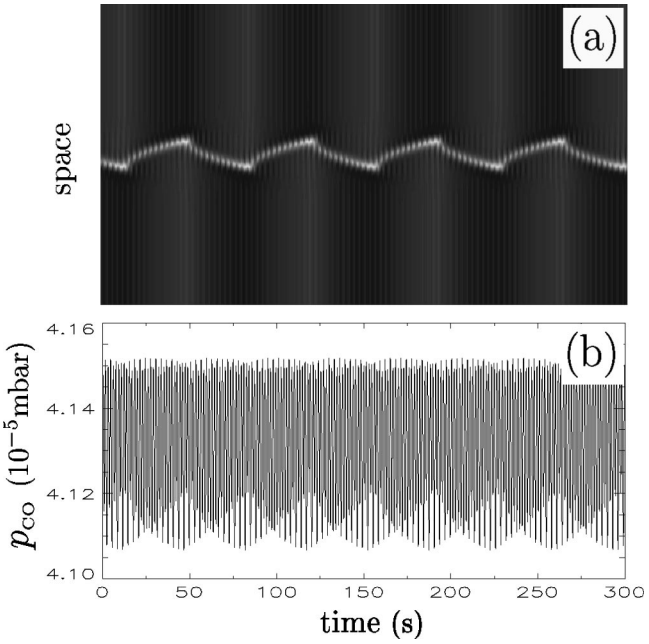

FIG. 13. (a) Space-time plot of front oscillations in a cluster pattern with no-flux boundaries. The oscillation amplitude R is plotted using a linear gray-scale map, with white color corresponding to the vanishing amplitude. (b) The respective quasiperiodic temporal variation of the feedback signal. The feedback parameters are $\tau/T_0=0.105$ and $\mu/p_{CO}^0=0.096$.

the numerical data close to the bifurcation point where front oscillations are harmonic. Hence, this is a supercritical Hopf bifurcation for the fronts. At larger distances from the bifurcation point, the front oscillations become strongly anharmonic and zigzag shaped, see Fig. 13(a). The spatial amplitude profile of such an oscillating front is time dependent. At the turning points of the front the amplitude R drops down and nearly vanishes. The control signal generated by two oscillating clusters becomes quasiperiodic after the Hopf bifurcation, see Fig. 13(b). The turning points of the phase front correspond to the points of maximal amplitude in the

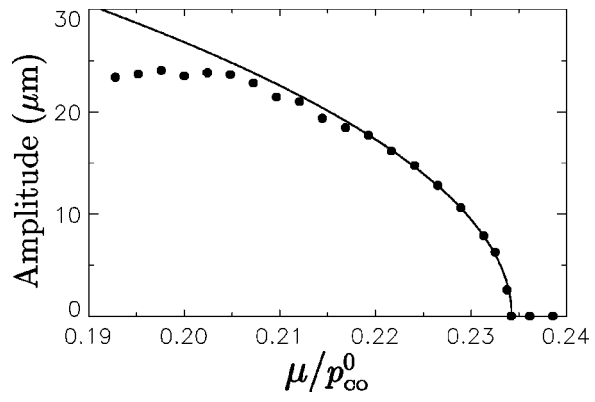

FIG. 14. Oscillation amplitude of a cluster front as a function of the feedback intensity. The data points are obtained numerically for a system size equal to 0.4 mm and no-flux boundary conditions. The solid line is a parabolic fit of the data points close to the bifurcation point. The delay time is kept constant, $\tau/T_0=0.105$.

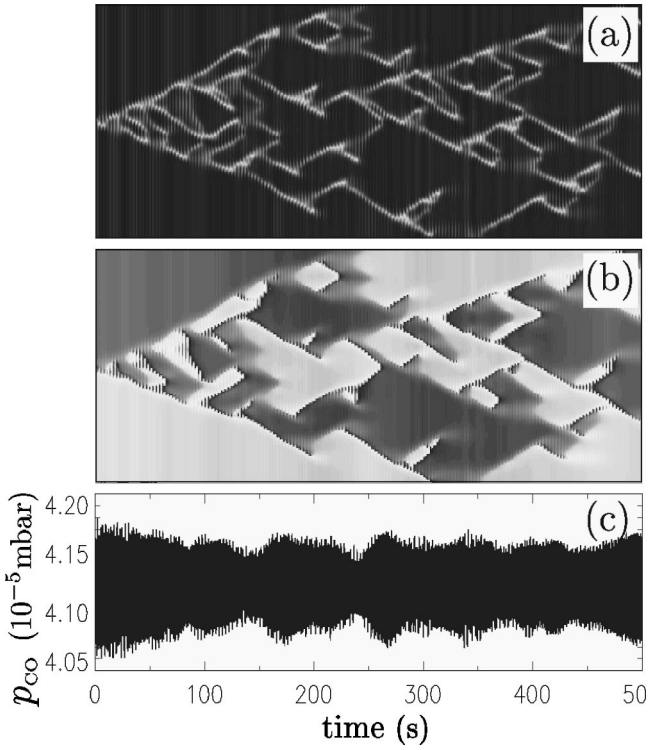

FIG. 15. Space-time plots of the reproduction cascade in a turbulent cluster pattern with no-flux boundaries. (a) Oscillation amplitude R and (b) phase ϕ in a time interval of 500 s. The phase distribution is displayed in a coordinate frame rotating with the period of the reference limit cycle. The corresponding chaotic feedback signal is shown in frame (c). The feedback parameters are $\tau/T_0=0.126$ and $\mu/p_{CO}^0=0.193$.

feedback oscillations. The change in the control signal provides a feedback on the phase front and hence is responsible for its turnaround. Note that the local oscillations in Fig. 13(a) are also slightly quasiperiodic due to the quasiperiodicity of the driving feedback signal. Though here the local amplitude differs slightly in the two oscillating cluster states, we still classify them as phase clusters because they smoothly originate from stationary phase clusters and their phase and amplitude properties are similar.

3. Cluster turbulence

Starting from strongly anharmonic front oscillations, a suitable change of feedback parameters leads to turbulent phase front behavior. An example of such irregular front behavior is shown in Fig. 15, where a front separating two π-shifted clusters branches out in a cascade of reproductions. The distribution of the oscillation amplitude is displayed in Fig. 15(a), and frame (b) shows the phase distribution in a rotating coordinate frame. The correspondent chaotic global oscillations are shown in frame (c). Such cluster turbulence does not spontaneously develop from a completely uniform oscillating state, i.e., a sufficiently strong local perturbation is needed to initiate the cascade. The fronts not only reproduce, but also can die out. Once initiated, the cluster turbulence can thus either spread over the whole medium, or die after some time.

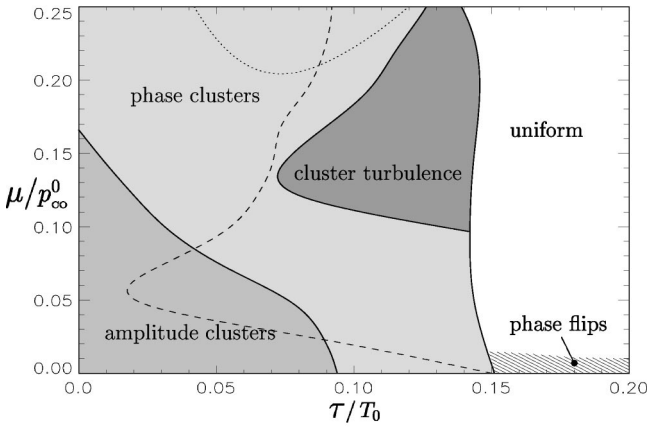

FIG. 16. Existence regions of different cluster patterns at small delay times.

The velocities of traveling fronts in this turbulent regime are almost constant. A front travels for some time, until an amplitude defect with vanishing amplitude R develops inside it. As a result, the front may split or die out. Phase fronts also sometimes emerge from smaller heterogeneities in the amplitude and the phase without directly originating from an amplitude defect. The irregular front behavior leads to turbulent deviations from the cluster states. Hence, the local oscillations are synchronous only inside cluster regions that were not visited by a front for several oscillation cycles.

To summarize our results on cluster patterns, we show in Fig. 16 the existence regions of different cluster patterns at small delays. We have found that the kind of the developing cluster pattern strongly depends on the initial and boundary conditions. The dashed line in Fig. 16 indicates the stability boundary of uniform oscillations with respect to small perturbations. On the right side from the dashed line both cluster patterns and uniform oscillations are possible, depending on the initial conditions. Note that cluster turbulence always coexists with uniform oscillations. The boundary conditions are important. For instance, in the region in the diagram where amplitude clusters are present, they were typically found for no-flux boundary conditions. For periodic boundary conditions, special initial conditions were needed here to obtain amplitude clusters, and traveling phase clusters are usually instead found. In the phase cluster region, for most parameter values the front behavior strongly depends on both the initial and the boundary conditions. Stationary phase clusters are only found above the dotted line in the diagram.

As already mentioned, traveling clusters require periodic boundary conditions that maintain the phase balance. For the same parameter values, no-flux boundaries either lead to the formation of stationary amplitude clusters as the asymptotic state, or to the front behavior shown in Fig. 17(a). When the first front collides with the left boundary, further movement of the second front would lead to phase imbalance. Instead, during a transient process, where in a part of the medium the oscillations strongly deviate from the former cluster states, a new cluster front is created. Again both clusters travel with constant velocity until the procedure repeats at the next front collision with the boundary. Figure 17(b) shows an example

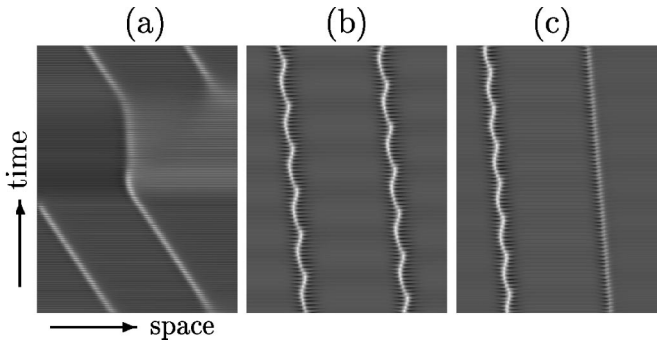

FIG. 17. Space-time plots of the amplitude in different cluster patterns. Traveling phase clusters (a) under no-flux boundary conditions, the time interval is 500 s. Drifting breathing clusters (b) and clusters with different behavior of the two fronts (c) in a system with periodic boundary conditions, each within the time interval of 200 s. The values of the parameters τ/T_0 and μ/p^0_{CO} are, respectively, (a) 0.114, 0.072, (b) 0.030, 0.193, and (c) 0.039, 0.193.

of breathing traveling clusters—this pattern develops when a traveling cluster undergoes a secondary Hopf bifurcation. As shown in Fig. 17(c), even more complex situations, where one of the fronts is steadily traveling and the other front is oscillating while traveling, are possible. The global oscillations of all three patterns in Fig. 17 are quasiperiodic.

V. FEEDBACK-INDUCED PATTERNS IN TWO SPACE DIMENSIONS

We have numerically explored feedback-induced pattern formation in Eqs. (1)–(4) also in two space dimensions. For the two-dimensional simulations we have chosen a slightly different CO pressure at vanishing feedback, $p^0_{\mathrm{CO}}=4.19\times10^{-5}$ mbar, in order to avoid a pressure drift into the regime of diffusion-induced turbulence, which in two dimensions occurs below $p_{\mathrm{CO}}\approx4.15\times10^{-5}$ mbar. The other parameters are as in the one-dimensional case, except for $u_{\mathrm{ref}}=0.4484$ that again corresponds to the unstable steady state. For the two-dimensional simulations, the natural period is $T_0=5.21$ s. No-flux boundary conditions are imposed at all boundaries.

Figure 18 shows four examples of different two-dimensional patterns. In the upper and lower rows we display spatial distributions of the oscillation phase and amplitude, respectively. In absence of feedback, uniform oscillations are stable, but a rotating spiral wave can be produced by an appropriate choice of the initial conditions, see Fig. 18(a). The oscillation amplitude vanishes in the spiral core and the phase changes continuously when traversing the spiral arms. By application of feedback and variation of its parameters, the spiral wave can be suppressed and uniform oscillations recovered (not shown). Phase-flip waves [Fig. 18(b)], asynchronous oscillation patterns [Fig. 18(c)], or (quasi-) stationary cluster patterns [Fig. 18(d)] could also be induced by appropriate feedbacks. The properties of uniform oscillations, phase flips, and desynchronized oscillations are similar to those of their one-dimensional counterparts.

The development of the asynchronous pattern in Fig. 18(c) from slightly perturbed uniform initial conditions leads to the breakdown of global oscillations. As in the one-

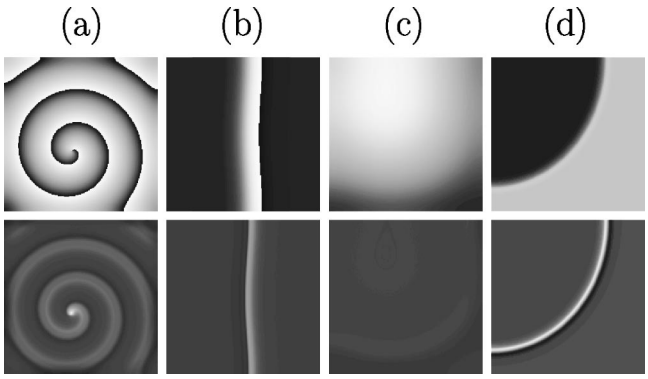

FIG. 18. Two-dimensional patterns: (a) a spiral wave in the absence of feedback, (b) a phase flip, (c) asynchronous oscillations, and (d) a cluster pattern. The snapshots of the oscillation phase (top row) and amplitude (bottom row) distributions are displayed in gray scale. The system size is 0.8×0.8 mm^2 for each pattern, except for the pattern (b) where it is 1.6×1.6 mm^2. The values of the parameters τ/T_0 and μ/p^0_{CO} are, respectively, (a) 0, 0, (b) 0.192, 0.010, (c) 0.768, 0.024, and (d) 0.067, 0.119.

dimensional case, the final asynchronous pattern is characterized by a constant amplitude and slow phase gradients. In the desychronization regime, the feedback cannot destroy spiral waves and they continue to represent a possible stable solution.

The phase cluster pattern in Fig. 18(d) consists of two π-shifted phase states separated by an almost stationary phase front. The clusters evolved from a nonuniform initial distribution. After the quick formation of the clusters, a slow drift of the front occurs, tending to minimize the front curvature while preserving the phase balance. The effect of the front curvature is the only essential difference compared to the corresponding one-dimensional stationary phase cluster pattern shown in Fig. 10(a). Stationary amplitude clusters were also observed in two-dimensional simulations and exhibited similar behavior as in the one-dimensional case.

After a bifurcation to traveling phase fronts, counter-propagating front parts can develop in a two-dimensional pattern (as previously noticed in externally forced oscillatory media [48]). The pattern developing under such conditions is shown in Fig. 19. The initial conditions in the upper and lower half of the originally straight front were chosen to correspond to the two branches of the pitchfork bifurcation, see Fig. 19(a). Because the two ends of the front propagate in opposite directions, a spiral wave develops in the central part

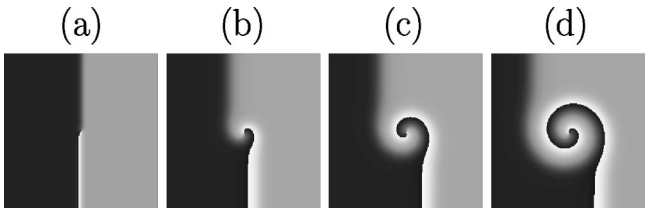

FIG. 19. Formation of a spiral wave from a cluster pattern with counter-propagating front parts. Consecutive snapshots of the oscillation phase ϕ are shown at equal time intervals of 96 s. The parameter values are $\tau/T_0=0.067$ and $\mu/p^0_{\mathrm{CO}}=0.024$.

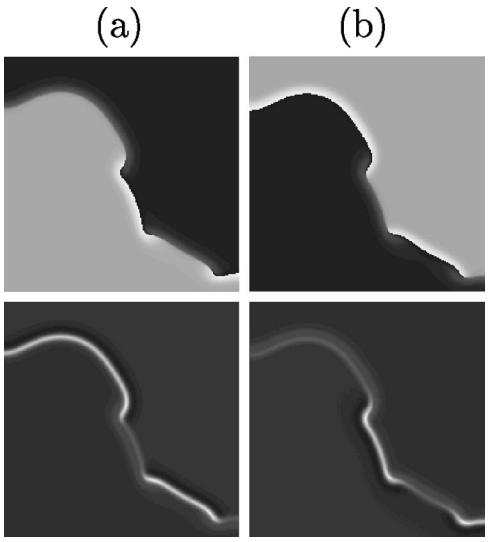

FIG. 20. Snapshots of the oscillation phase (top row) and amplitude (bottom row) distribution in a cluster pattern with time-dependent front profile. The time interval between the snapshots (a) and (b) is half of the oscillation period in the clusters. The parameter values are $\tau/T_0=0.067$ and $\mu/p^0_{\mathrm{CO}}=0.072$.

[Fig. 19(b)–19(d)], and later spreads out over the whole medium. This process is accompanied by the breakdown of the global oscillations. As the spiral grows, the fraction of the medium occupied by the fronts with rapid phase variation slowly increases at the expense of the areas occupied by the two uniform phase states. Eventually they become too small to generate a feedback signal sufficient to maintain the clusters. Therefore, the nonequilibrium Ising-Bloch bifurcation provides an additional scenario for the breakdown of the global feedback. The final state is characterized by a spiral wave with continuous phase distribution and nearly vanishing global oscillations, as in absence of global feedback.

The pattern displayed in Fig. 20 was obtained with feedback parameters corresponding to the case of cluster front oscillations in one space dimension. A nonuniform phase and amplitude distribution was taken as initial condition. The frames (a) and (b) show the phase (top row) and amplitude (bottom row) distributions at time moments separated by half the oscillation period. Instead of front oscillations, which are seen in this case in the one-dimensional system and are accompanied by quasiperiodic variations of the global control signal, a different kind of pattern is observed in two dimensions. The area occupied by each of the clusters in Fig. 20 is almost balanced and no significant oscillations of the fronts take place. The global oscillations are almost periodic here. The front separating the two clusters is broken into parts (see the bottom row in Fig. 20). As time goes on, the amplitudes in different front parts periodically drop down at opposite oscillation phases. On a large time scale of several hundred oscillation periods, weak drift of the clusters and slow gradual variation of their shapes are observed. The splitting of the front into different parts is a two-dimensional phenomenon that is typically observed starting from nonuniform initial conditions. However, if a simulation is started with a straight front, it remains stable with respect to small pertur-

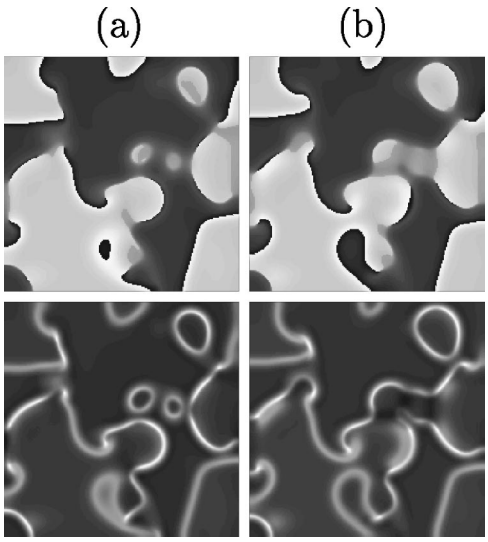

FIG. 21. Turbulent cluster pattern. The two consecutive snapshots of the oscillation phase (top row) and amplitude (bottom row) distributions are separated by a time interval of two oscillation periods. The parameter values are $\tau/T_0=0.067$ and $\mu/p_{\mathrm{CO}}^0=0.024$.

bations and shows periodic oscillations, as in the corresponding one-dimensional case.

When cluster fronts show irregular motion in one space dimension, the respective two-dimensional clusters also exhibit complex turbulent evolution. As an example, two subsequent snapshots of a turbulent cluster pattern are shown in Fig. 21 (top and bottom rows again correspond to the phase and amplitude distributions). Each cluster consists of different patches that continuously vary their shape while the separating fronts propagate through the medium. The front propagation occurs at an almost constant velocity in the planar front parts. Turbulence is maintained in this system through repeated popping up of bubblelike domains with the opposite phase in the region occupied by any of the two phase clusters. These bubbles or spots grow for a few oscillation cycles and eventually merge with the larger cluster patches. On the other hand, cluster patches can also shrink and disappear. New cluster spots usually originate at the locations that were previously visited by the fronts, where amplitude and phase heterogeneities were left. Uniform oscillations are stable in this parameter region and to initiate a turbulent cascade, sufficiently strong local perturbations must be applied to the uniform state.

VI. DISCUSSION

We have shown by means of numerical simulations of a realistic model that pattern formation in the catalytic CO oxidation can be effectively controlled by implementation of a delayed global feedback. Even though the applied feedback is global, it allows one to control spatial features by the appropriate choice of the feedback parameters. In the case under study, when uniform oscillations are stable in absence of feedback, variation of the feedback intensity and the delay time allows us to produce various structures, including phase flips, asynchronous oscillations, and different kinds of cluster patterns.

In addition to the model calculation results we have presented an empirical variable transformation technique that makes possible a time-resolved phase and amplitude characterization of anharmonically oscillating patterns. This technique also allows a direct comparison to previous studies of delayed global feedback control based on the normal form approach. The properties of the phase flips and the desynchronization breakdown of the global oscillations observed in our numerical observations are in good agreement with previous studies of the globally coupled CGLE [31,33]. The observed amplitude clusters resemble the respective cluster solutions in the frame of the amplitude equation [45]. Stationary two-phase clusters are similar to those found for the photosensitive Belousov-Zhabotinsky reaction [26] under global feedback in absence of a time delay. Traveling and oscillating two-phase clusters represent, as far as we know, new kinds of patterns induced through the action of global feedback. We have also found cluster turbulence that represents another interesting example of complex spatiotemporal behavior induced by global delayed feedbacks. The turbulent formation of cluster spots is different from the birth of spots through self-replication that was previously reported in bistable systems [49].

Though our systematic study of feedback-induced patterns has been conducted using a particular model of a surface chemical reaction, we expect that such phenomena are typical for many reaction-diffusion systems in the presence of delayed global feedbacks. Indeed, some two-phase cluster patterns have been recently observed in experiments with the light-sensitive Belousov-Zhabotinsky reaction under global feedback without time delay [25] and under external forcing [6,8]. The experiments with artificial global feedbacks in surface chemical reactions are in progress.

ACKNOWLEDGMENTS

We acknowledge financial support of the Deutsche Forschungsgemeinschaft in the framework of the Sonderforschungsbereich 555 ''Complex Nonlinear Processes.'' We thank K. Showalter and A. von Oertzen for interesting discussions.

[1] Y. Kuramoto, *Chemical Oscillations, Waves and Turbulence* (Springer, Berlin, 1984).
[2] A. S. Mikhailov, *Foundations of Synergetics I* (Springer, Berlin, 1990).
[3] D. Walgraef, *Spatio-Temporal Pattern Formation* (Springer, New York, 1997).
[4] P. Coullet and K. Emilsson, Physica D **61**, 119 (1992).
[5] A. Schrader, M. Braune, and H. Engel, Phys. Rev. E **52**, 98

(1995).
[6] V. Petrov, Q. Ouyang, and H. L. Swinney, Nature (London) **388**, 655 (1997).
[7] H. Chaté, A. Pikovsky, and O. Rudzick, Physica D **131**, 17 (1999).
[8] A. L. Lin, M. Bertram, K. Martinez, H. L. Swinney, A. Ardelea, and G. F. Carey, Phys. Rev. Lett. **84**, 4240 (2000).
[9] E. Ott, C. Grebogi, and J. A. Yorke, Phys. Rev. Lett. **64**, 1196 (1990).
[10] K. Pyragas, Phys. Lett. A **170**, 421 (1992).
[11] J. E. S. Socolar, D. W. Sukow, and D. J. Gauthier, Phys. Rev. E **50**, 3245 (1994).
[12] H. Gang and H. Kaifen, Phys. Rev. Lett. **71**, 3794 (1993).
[13] I. Aranson, H. Levine, and L. Tsimring, Phys. Rev. Lett. **72**, 2561 (1994).
[14] W. Lu, D. Yu, and R. G. Harrison, Phys. Rev. Lett. **76**, 3316 (1996).
[15] M. E. Bleich and J. E. S. Socolar, Phys. Rev. E **54**, R17 (1996).
[16] R. Martin, A. J. Scroggie, G.-L. Oppo, and W. J. Firth, Phys. Rev. Lett. **77**, 4007 (1996).
[17] D. Battogtokh and A. Mikhailov, Physica D **90**, 84 (1996).
[18] M. E. Bleich, D. Hochheiser, J. V. Moloney, and J. E. S. Socolar, Phys. Rev. E **55**, 2119 (1997).
[19] M. Münkel, F. Kaiser, and O. Hess, Phys. Rev. E **56**, 3868 (1997).
[20] R. O. Grigoriev, M. C. Cross, and H. G. Schuster, Phys. Rev. Lett. **79**, 2795 (1997).
[21] S. Sinha and N. Gupte, Phys. Rev. E **58**, R5221 (1998).
[22] S. Boccaletti, D. Maza, H. Mancini, R. Genesio, and F. T. Arecchi, Phys. Rev. Lett. **79**, 5246 (1997).
[23] Th. Pierre, G. Bonhomme, and A. Atipo, Phys. Rev. Lett. **76**, 2290 (1996).
[24] G. Franceschini, S. Bose, and E. Schöll, Phys. Rev. E **60**, 5426 (1999).
[25] V. K. Vanag, L. Yang, M. Dolnik, A. M. Zhabotinsky, and I. R. Epstein, Nature (London) **406**, 389 (2000).
[26] L. Yang, M. Dolnik, A. M. Zhabotinsky, and I. R. Epstein, Phys. Rev. E **62**, 6414 (2000).
[27] S. Grill, V. S. Zykov, and S. C. Müller, Phys. Rev. Lett. **75**, 3368 (1995).
[28] V. S. Zykov, A. S. Mikhailov, and S. C. Müller, Phys. Rev. Lett. **78**, 3398 (1997).
[29] K. Krischer and A. S. Mikhailov, Phys. Rev. Lett. **73**, 3165 (1994).
[30] D. Battogtokh, M. Hildebrand, K. Krischer, and A. S. Mikhailov, Phys. Rep. **288**, 235 (1997).
[31] F. Mertens, R. Imbihl, and A. Mikhailov, J. Chem. Phys. **99**, 8668 (1993).
[32] F. Mertens, R. Imbihl, and A. Mikhailov, J. Chem. Phys. **101**, 9903 (1994).
[33] D. Battogtokh, A. Preusser, and A. Mikhailov, Physica D **106**, 327 (1997).
[34] H. H. Rotermund, Surf. Sci. Rep. **29**, 265 (1997).
[35] S. Jakubith, H. H. Rotermund, W. Engel, A. v. Oertzen, and G. Ertl, Phys. Rev. Lett. **65**, 3013 (1990).
[36] R. Imbihl and G. Ertl, Chem. Rev. **95**, 697 (1995).
[37] B. P. Belousov, in *Oscillations and Traveling Waves in Chemical Systems*, edited by R. J. Field and M. Burger (Wiley, New York, 1985), p. 605.
[38] R. Imbihl and G. Veser, J. Vac. Sci. Technol. A **12**, 2170 (1994).
[39] A. v. Oertzen, H. H. Rotermund, A. S. Mikhailov, and G. Ertl, J. Phys. Chem. B **104**, 3155 (2000).
[40] K. Krischer, M. Eiswirth, and G. Ertl, J. Chem. Phys. **96**, 9161 (1992).
[41] M. Bär, M. Eiswirth, H. H. Rotermund, and G. Ertl, Phys. Rev. Lett. **69**, 945 (1992).
[42] M. Bär, N. Gottschalk, M. Eiswirth, and G. Ertl, J. Chem. Phys. **100**, 1202 (1994).
[43] A. v. Oertzen, A. S. Mikhailov, H. H. Rotermund, and G. Ertl, J. Phys. Chem. B **102**, 4966 (1998).
[44] M. Falcke and H. Engel, J. Chem. Phys. **101**, 6255 (1994).
[45] M. Falcke, H. Engel, and M. Neufeld, Phys. Rev. E **52**, 763 (1995).
[46] M. Falcke and H. Engel, Phys. Rev. E **56**, 635 (1997).
[47] M. C. Cross and P. C. Hohenberg, Rev. Mod. Phys. **65**, 851 (1993).
[48] P. Coullet, J. Lega, B. Houchmanzadeh, and J. Lejzerowicz, Phys. Rev. Lett. **65**, 1352 (1990).
[49] K.-J. Lee, W. D. McCormick, J. E. Pearson, and H. L. Swinney, Nature (London) **369**, 215 (1994).
[50] V. Petrov, S. Metens, P. Borckmans, G. Dewel, and K. Showalter, Phys. Rev. Lett. **75**, 2895 (1995).